Inorganic Chemistry
Article
pubs.acs.org/IC

Three-Dimensionality of Electronic Structures and Thermoelectric Transport in $SrZrN_2$ and $SrHfN_2$ Layered Complex Metal Nitrides

Isao Ohkubo* and Takao Mori

WPI Research Center, International Center for Materials Nanoarchitectonics, National Institute for Materials Science, 1-1 Namiki, Tsukuba, Ibaraki 305-0044, Japan

Ⓢ *Supporting Information*

ABSTRACT: Layered materials have several properties that make them suitable as high-performance thermoelectric materials. In this study, we focus on the complex metal nitrides $SrZrN_2$ and $SrHfN_2$, which have an α-$NaFeO_2$ layered crystal structure. To determine their electronic band structure features and potential thermoelectric transport properties, we calculated the electronic band structures and electronic transport coefficients for $SrZrN_2$ and $SrHfN_2$ using density-functional theory and Boltzmann transport theory, respectively. Despite the layered crystal structure, $SrZrN_2$ and $SrHfN_2$ both had three-dimensional electronic structures and isotropic electronic transport because of the contribution of the Sr $4d_{x^2-y^2} + 4d_{xy}$ orbitals to the bottom of the conduction bands in addition to that of the Zr $4d_{z^2}$ (Hf $5d_{z^2}$) orbital. The three-dimensional electronic structures predict the appearance of large Seebeck coefficients ($-145\ \mu V\ K^{-1}$ at 300 K, $-370\ \mu V\ K^{-1}$ at 1200 K) and large electronic thermoelectric figures of merit.

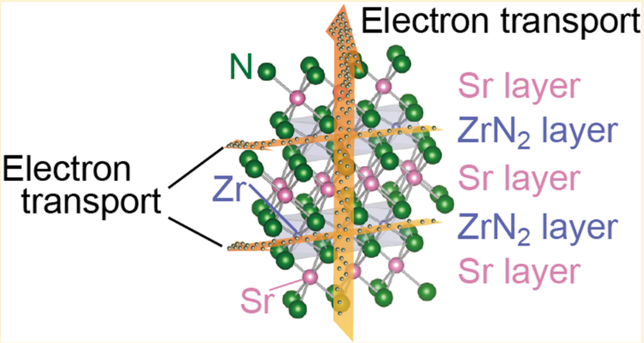

INTRODUCTION

Layered materials are particularly interesting because of their unusual electronic and physical properties, such as thermoelectric transport,[1] superconductivity,[2,3] and ionic conduction.[4] Layered materials with α-$NaFeO_2$ and other related layered crystal structures (Figure 1a) are particularly important, because they are used for energy generation and saving applications. For example, Na_xCoO_2 exhibits excellent thermoelectric properties[5] and is a base material for superconductors,[6] and $LiCoO_2$ is used as a cathode material in lithium ion batteries.[4] α-$NaFeO_2$ materials have quasi-two-dimensional electronic structures and exhibit anisotropic transport,[5,7,8] which results in superconductivity and a large thermoelectric effect. Although there are many complex metal oxides with α-$NaFeO_2$ crystal structures, other types of compounds are less well-known. $SrZrN_2$ and $SrHfN_2$ are complex metal nitrides with an α-$NaFeO_2$ crystal structure (Figure 1a).[9] Complex metal nitrides with layered crystal structures include an extensive range of compounds with diverse chemistry.[10] Some layered complex metal nitrides, such as MNX (M = Ti, Zr, Hf; X = Cl, Br, I)[11] and ternary transition-metal dinitrides AMN_2 (A = alkaline earth metal; M = Ti, Zr, Hf),[1] are superconducting with high critical temperatures. Although $SrZrN_2$ and $SrHfN_2$ have been synthesized and their structures characterized, their physical properties and electronic structures are still unknown. In the present study, we calculated the electronic structure and transport of $SrZrN_2$ and $SrHfN_2$ by using density-functional theory (DFT) and Boltzmann transport theory to evaluate their electronic structure and transport properties, particularly the thermoelectric transport.

COMPUTATIONAL METHODS

Our calculations are based on DFT using the full-potential linearized augmented plane wave approach, as implemented in the WIEN2k code.[12] The modified Becke-Johnson (mBJ)[13] exchange and correlation functional was adopted because it produces energy band gaps (E_g's) for semiconductors and insulators that are closer to experimental values than the generalized gradient approximation/Perdew−Burke−Ernzerhof (GGA/PBE) functional and local density approximation.[14] The E_g value of 2.75 eV in $SrTiO_3$ calculated using the mBJ exchange and correlation functional is closer to the experimental E_g value of 3.2 eV than the E_g value of 1.9 eV calculated using the GGA/PBE functional.[14−16] The size of the basis set is controlled by the parameter $R_{mt}K_{max}$, where K_{max} is the plane wave cutoff and R_{mt} is the smallest muffin-tin radius. It is set to a high value of 7.0 for all materials. The electronic structure is calculated using 100 $\boldsymbol{k}$-points in the Brillouin zone. Convergences are achieved with $\boldsymbol{k}$-point sampling of 100. We use 40 000 $\boldsymbol{k}$-points for the transport calculations. The transport properties are calculated by semiclassical Boltzmann transport theory with the constant scattering approximation and the rigid band approach,[17,18] as implemented in the BoltzTraP code.[19] In this DFT calculation, we use structural coordinates and lattice parameters taken from X-ray diffraction measurements.[9] $SrZrN_2$ and $SrHfN_2$ crystallize in the hexagonal space group $R\bar{3}m$, of which α-$NaFeO_2$ is a typical example.[9] The measured lattice constants are a = 3.373 Å and c = 17.676 Å for $SrZrN_2$, and a = 3.345 Å and c = 17.678 Å for $SrHfN_2$. Figure 1a shows the alternate stacking of the MN_2 (M =

Received: April 16, 2014
Published: August 6, 2014

dx.doi.org/10.1021/ic500902q | *Inorg. Chem.* 2014, 53, 8979−8984

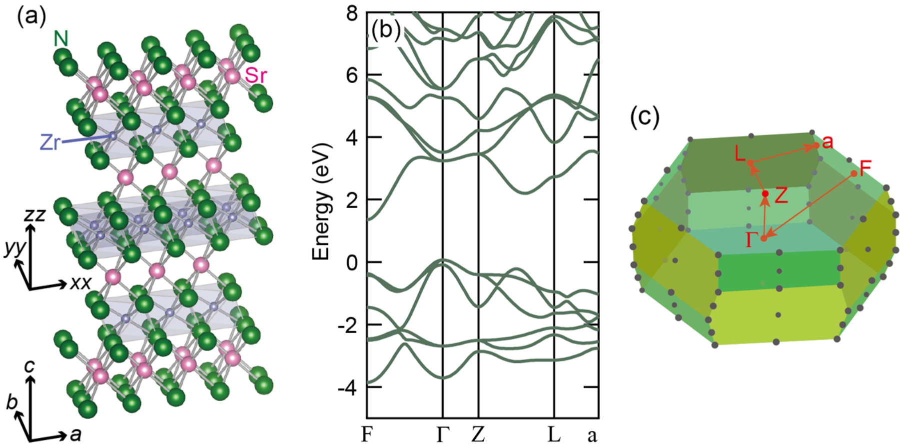

Figure 1. Crystal structure and electronic band structure of $SrZrN_2$ with an α-$NaFeO_2$ layered crystal structure. (a) Crystal structure, (b) electronic band structure, and (c) Brillouin zones for the α-$NaFeO_2$ layered structure. The labels in the Brillouin zones, Γ, L, F, Z, and a, correspond to 0, 0, 0; 1/2, 0, 0; 1/2, 1/2, 0; 1/2, 1/2, 1/2; and 0.65756, 0.34244, 0, respectively, in lattice constant units.

Zr, Hf) layer and the Sr layer along the *c* axis. The face-sharing octahedral Zr−N and Hf−N anions are composed of a Zr or Hf ion coordinated to six equidistant nitrogens. Details of the calculation conditions are provided in the Supporting Information.

RESULTS AND DISCUSSION

Figures 1b and S1 (Supporting Information) show the electronic band structures of $SrZrN_2$ and $SrHfN_2$. Both $SrZrN_2$ and $SrHfN_2$ are band insulators with calculated band gaps (E_g) of 1.29 and 1.37 eV, respectively. These are slightly smaller than those of $SrTiN_2$ (E_g = 1.55 eV), $BaZrN_2$ (1.59 eV), and $BaHfN_2$ (1.68 eV), which have a $KCoO_2$ layered structure.[16] The top of the valence band and the bottom of the conduction band are located at the Γ and F points, respectively. Given that calculated band gaps are often underestimated, even if the mBJ exchange and correlation functional improve the values of energy band gaps, the true gaps of $SrZrN_2$ and $SrHfN_2$ may be much larger. The lowest conduction band in $SrZrN_2$ has a primarily Zr $4d_{z^2}$ and $4d_{xz}$ + $4d_{yz}$ orbital character and a width of 2 eV. The main contribution to the bottom of the conduction band at the F point is from both the Zr $4d_{z^2}$ orbital and the Sr $4d_{x^2-y^2}$ + $4d_{xy}$ orbital. The Zr 4d and Sr 4d characters extend between 6 and 9 eV from the conduction band minimum, partially because of the crystal-field splitting of the 4d orbitals. The highest valence band has an N 2p character. Because the Zr 4d and Sr 4d states are empty, Zr and Sr are in the 4+ and 2+ states, respectively. The rest of the electronic structure indicates a closed shell ionic insulator with some mixing of N 2p states and Zr 4d and Sr 4d states, analogous to the mixing in other ionic compounds. Figure S1 (Supporting Information) shows that the band characters of $SrHfN_2$ are similar to those of $SrZrN_2$. The band dispersions of the lowest conduction band and the highest valence band along the Γ-Z direction (corresponding to the *c* axis) in $SrZrN_2$ and $SrHfN_2$ seem to be much lower than those for the other in-plane directions. The bottom of the conduction band and the top of the valence band are located at the F and Γ points, where the band dispersions are much larger than those for the Γ-Z direction. The effective masses (m^*) in $SrZrN_2$ at the bottom of conduction band (F-point) are 0.305 m_0 (*c* axis direction, m_c^*), 0.407 m_0 (longitudinal direction, F−Γ, $m_{\parallel}^*$), and 0.271 m_0 (transverse direction, F−a, $m_{\perp}^*$). Here, m_0 is the free electron mass. Similarly, the values of m^* in $SrHfN_2$ at the bottom of the conduction band (F-point) are 0.298 m_0 (m_c^*), 0.406 m_0 ($m_{\parallel}^*$), and 0.263 m_0 ($m_{\perp}^*$). The values of m^* in $SrZrN_2$ at the top of the valence band (F-point) are 0.734 m_0 (m_c^*), 0.504 m_0 ($m_{\parallel}^*$), and 0.580 m_0 ($m_{\perp}^*$). The values of m^* in $SrHfN_2$ at the top of the valence band (F-point) are 0.791 m_0 (m_c^*), 0.523 m_0 ($m_{\parallel}^*$), and 0.596 m_0 ($m_{\perp}^*$). These effective masses were calculated from a parabolic fitting of the dispersion very near the conduction band minima using the principal axes of the ellipsoids. Regardless of the direction, the effective masses in $SrZrN_2$ and $SrHfN_2$ were the same order of magnitude. In thermoelectric selenides and tellurides, such as PbSe and GeTe, the effective masses along the transverse direction are an order of magnitude larger than those along the longitudinal direction, indicating large anisotropic electronic structures.[20] Therefore, $SrZrN_2$ and $SrHfN_2$ may be a three-dimensional system rather than two-dimensional system.

Figure 2 shows several calculated transport properties for $SrZrN_2$ at 300 K, plotted as a function of chemical potential (μ). To estimate the efficiency of the material, we use the electronic dimensionless thermoelectric figure of merit, $S^2\sigma T/\kappa_e$ (=Z_eT),[21] and compare it with that of $SrTiO_3$, which is a well-known compound with good thermoelectric properties, because the lattice thermal conductivity cannot be calculated by DFT in the usual way. The Seebeck coefficient, electrical conductivity, and the electronic part of the thermal conductivity of a compound can be estimated on the basis of the compound's band structure. The relaxation time, τ, is constant in this work. Although the electrical conductivity and power factor are calculated with respect to τ, the Seebeck coefficient is independent of τ. This approach has been used to evaluate the electrical transport properties of thermoelectric compounds, in addition to the rigid band approach.[17,18] The electronic conductivities, electronic part of the thermal conductivities, Seebeck coefficients, thermoelectric power factors, and electronic dimensionless thermoelectric figures of merit are shown for the *xx* and *zz* directions, which correspond to the in-plane direction along the ZrN_2 layer and the direction perpendicular to the layers along the *c* axis, respectively. We have previously reported highly anisotropic electronic structures and transport coefficients in $SrTiN_2$, $BaZrN_2$, and $BaHfN_2$, which have $KCoO_2$ layered crystal structures.[16] The in-plane electronic transport in these materials was much larger than the out-of-plane electronic transport. However, it initially

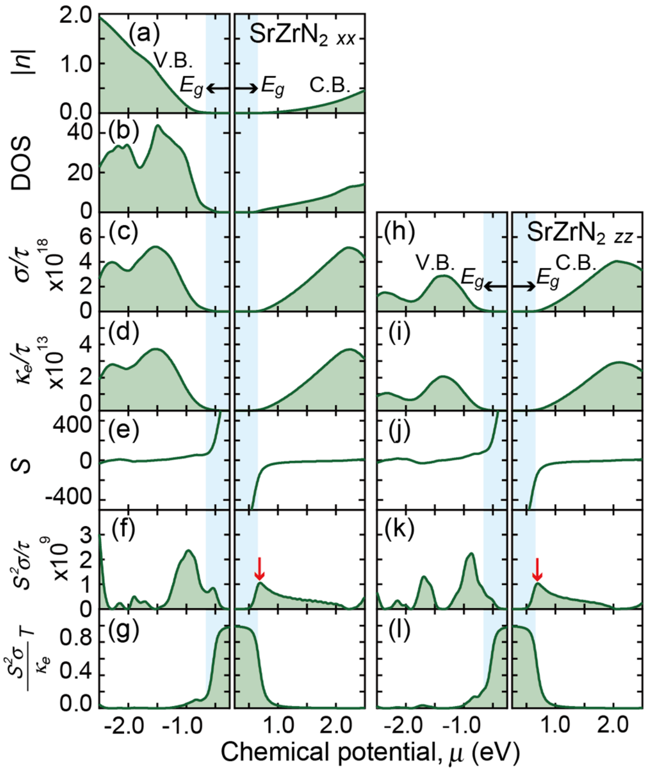

Figure 2. Absolute values of carrier concentrations (|n|), density of states (DOS), and xx and zz direction transport coefficients for SrZrN$_2$ versus the chemical potential (μ) at 300 K. (a) Absolute values of carrier concentrations, (b) DOS, (c and h) electronic conductivities (σ/τ), (d and i) electronic part of the thermal conductivities (κ_e/τ), (e and j) Seebeck coefficients (S_{xx}), (f and k) power factors ($S^2\sigma/\tau$), and (g and l) electronic dimensionless figures of merit (Z_eT). Left and right panels show the valence band side (V.B.) and conduction band side (C.B.), respectively. The arrows indicate the peak in the power factor near the bottom of the C.B. (a−g) Carrier concentration, DOS, and xx direction transport coefficients, and (h−l) zz direction transport coefficients, respectively. The units for carrier concentration, DOS, σ/τ, κ_e/τ, S, and power factor ($S^2\sigma/\tau$), are f.u.$^{-1}$, states eV^{-1} f.u.$^{-1}$, Ω^{-1} cm^{-1} s^{-1}, W cm^{-1} K^{-1} s^{-1}, μV K^{-1}, and W cm^{-1} K^{-2} s^{-1}, respectively, where f.u. stands for formula unit.

appears that the transport in SrZrN$_2$ is not anisotropic; the xx direction transport properties appear to be similar to those for the zz direction. SrHfN$_2$ also shows properties similar to those of SrZrN$_2$ (Figure S2, Supporting Information). The electronic band structures in SrZrN$_2$ and SrHfN$_2$ are three-dimensional, and thus, electronic conductivities are expected to be similar in both the zz direction and the xx direction.

The doping levels represented in the full range of the plots may not be achievable in practice; however, they allow a complete analysis of what produces good electronic properties and thermoelectric efficiency.[19,22] In the rigid-band approach, the positive and negative chemical potentials correspond to n and p doping, respectively. The Seebeck coefficients reach a maximum near the middle of the energy band gaps (E_g), because the Seebeck coefficient in semiconductors is inversely proportional to the carrier concentration. However, in the case of n-type semiconductors, the doping level should be controlled around the bottom of the conduction band. SrZrN$_2$ and SrHfN$_2$ may be n-type semiconductors, because most compounds containing Zr^{4+} and Hf^{4+} (d^0) ions are n-type semiconductors.[23] Experimentally, the doping level in n-type semiconductors can be controlled around the bottom of the conduction band. Under the rigid band approximation, the chemical potential varies in addition to the carrier concentration. To achieve the maximum power factor, the chemical potentials should be near the bottom of the conduction band. Both the xx and zz direction power factors of SrZrN$_2$ reach their maximum at 0.045 eV in the SrZrN$_2$ conduction band (arrows in Figure 2f,k). Similarly, the xx and zz direction maximum power factors in SrHfN$_2$ are at 0.015 eV in the conduction band (Figure S2, Supporting Information). In general, the power factor ($S^2\sigma$) depends on the carrier concentration. Figures 3 and S3 (Supporting Information) show the Seebeck coefficient (S) and power factors plotted as a function of logarithmic carrier concentration. The Seebeck coefficients show a logarithmic dependence on carrier concentrations, which is consistent with Pisarenko behavior. The power factor in SrZrN$_2$ reaches its maximum value at a carrier density of 2.3×10^{19} cm^{-3}, corresponding to 0.0015 electrons per Zr site, and in SrHfN$_2$ at 8.2×10^{18} cm^{-3}, corresponding to 0.0014 electrons per Hf site. In the n-type semiconductor SrTiO$_3$, the electron carrier concentration is controlled by substituting La^{3+} ions into the Sr^{2+}-site and Nb^{5+} ions into the Ti^{4+}-site.[24,25] Thus, the carrier concentrations in SrZrN$_2$ and SrHfN$_2$ may be controlled by similar substitution by La^{3+}, for example.

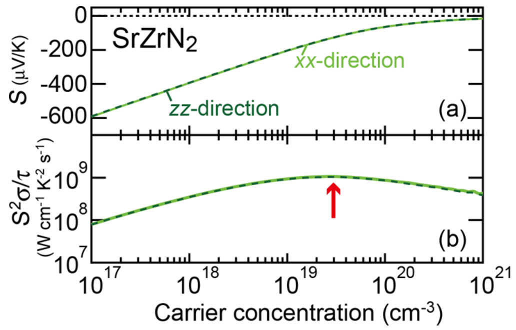

Figure 3. Carrier concentration dependences of (a) Seebeck coefficients (S) and (b) power factors ($S^2\sigma/\tau$) in SrZrN$_2$ at 300 K. Red arrows indicate carrier concentrations where the maximum power factor values are achieved.

The transport properties were evaluated on the basis of the rigid band approximation, in which the electronic structure of the material is expected to remain unchanged in the carrier doped regions. To express the results using a more tangible quantity, it is necessary to obtain the chemical potential from the carrier concentration. We have calculated the carrier concentration in terms of chemical potential (μ) for each temperature by using

$$n = \int D_e(E) \frac{1}{e^{(\mu - E)/k_B T} + 1}\, dE \qquad (1)$$

In this equation, n is the carrier concentration, E is the energy, D_e is the DOS obtained from the electronic structure calculation, k_B is the Boltzmann constant, and T is the temperature. Figures 4 and S4 (Supporting Information) show the calculated chemical potentials of SrZrN$_2$ and SrHfN$_2$, respectively. The chemical potentials of both compounds are located in the band gap for low carrier concentrations of less than 10^{19} cm^{-3}. At carrier concentrations greater than 10^{20} cm^{-3}, the chemical potentials are located in the conduction

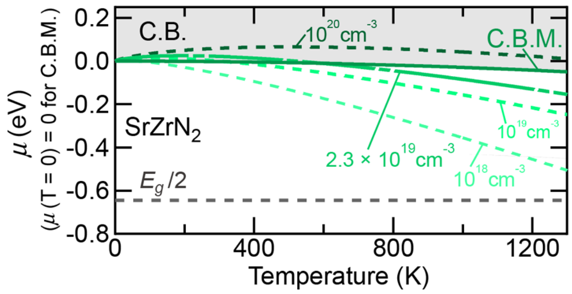

Figure 4. Variation of chemical potential, μ, as a function of temperature for SrZrN$_2$. The gray regions indicate the conduction band (C.B.). The solid lines indicate the conduction band minimum (C.B.M.).

band, which indicates that SrZrN$_2$ and SrHfN$_2$ behave as degenerate semiconductors.

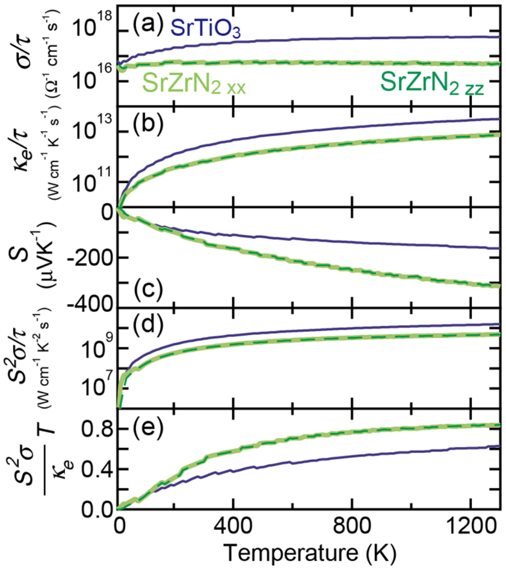

Figure 5. Temperature dependence of the transport properties of (blue lines) SrTiO$_3$ and (green lines) SrZrN$_2$ at electron carrier concentrations (M^{-1}, M = Ti, Zr) of 0.04 (6.2 × 10^{20} cm^{-3}) for SrTiO$_3$ and 0.0015 (2.3 × 10^{19} cm^{-3}) for SrZrN$_2$. (a) Electronic conductivities, (b) electronic part of the thermal conductivities, (c) Seebeck coefficients, (d) power factors, and (e) electronic dimensionless figures of merit (Z_eT). The labels (light green line) *xx* and (dashed green line) *zz* indicate the in-plane and out-of-plane transport properties along the *c* axis.

Figures 5 and S5 (Supporting Information) show the temperature dependences of several calculated transport coefficients of SrZrN$_2$ and SrHfN$_2$, respectively. Both SrZrN$_2$ and SrHfN$_2$ may be stable at temperatures above 1000 K because they are synthesized at 1000 °C.[9] The transport coefficients were calculated at carrier concentrations of 0.0015 per Zr-site, corresponding to 2.3 × 10^{19} cm^{-3} (SrZrN$_2$), and 0.0015 per Hf-site, corresponding to 8.2 × 10^{18} cm^{-3} (SrHfN$_2$), at which the maximum power factors were obtained. Figures 5 and S5 (Supporting Information) also show the calculated transport coefficients of SrTiO$_3$ for comparison, because it is a three-dimensional perovskite with good thermoelectric properties. The transport coefficients of SrTiO$_3$ are the same as those in ref 16, and are calculated with an electron carrier concentration of 0.04 per Ti-site, corresponding to 6.7 × 10^{20} cm^{-3}, to achieve the maximum thermoelectric power factor. Our calculations produce appropriate values for the transport coefficients in SrTiO$_3$. Our calculated Seebeck coefficient for SrTiO$_3$ at the carrier concentration of 6.7 × 10^{20} cm^{-3} is −120 μV K^{-1} at 300 K, which is similar to the experimentally determined (−150 to −170 μV K^{-1})[24,25] and previously reported calculated (−100 to −150 μV K^{-1}) values.[26,27] The transport properties of SrZrN$_2$ and SrHfN$_2$ can be compared directly with those of SrTiO$_3$ because the calculation method and procedures are the same. Figure 5 and S5 (Supporting Information) clearly show that the estimated transport properties of SrZrN$_2$ and SrHfN$_2$ are not anisotropic, with the in-plane *xx* and *yy* direction transports are very similar to that in the *zz* direction. As shown in Figure S6 (Supporting Information), the conductivity ratios σ_{xx}/σ_{zz} in SrZrN$_2$ and SrHfN$_2$ are around 1 and are very low compared with those of other layered compounds, such as SrTiN$_2$ (σ_{xx}/σ_{zz} ~ 7300 at 10 K, 13 700 at 300 K),[16] La$_{2-x}$Sr$_x$CuO$_4$ (σ_{xx}/σ_{zz} ~ 100−300 at 300 K),[28] and Na$_x$CoO$_2$ (σ_{xx}/σ_{zz} ~ 200 at 4.2 K).[5,8] This is interesting, considering that the MN$_2$ layer has bonds in the *xx* and *yy* directions only. The nearest neighbor M−N bonds and the second neighbor M−M bonds are formed along the *yy* and *xx* directions, respectively. The transport coefficients are the same for the *xx* and *yy* directions, despite the difference in bonding. Experimentally, anisotropic electronic transport has been reported in Na$_x$CoO$_2$, which has an α-NaFeO$_2$ crystal structure.[5,8] The electronic conductivity in the *xx* direction in Na$_x$CoO$_2$ is significantly larger than that in the *zz* direction. The anisotropic transport in Na$_x$CoO$_2$ is consistent with the electronic band structure calculations, which show a large cylindrical hole Fermi surface in the k_z direction, perpendicular to the layer, indicating a quasi-two-dimensional electronic structure and larger in-plane electronic transport.[7] The conductive octahedral CoO$_2$ layer isolated by a Na layer also contributes to the anisotropic transport. In contrast, the constant energy surfaces at the electron carrier concentrations required to achieve maximum power factors for SrZrN$_2$ and SrHfN$_2$ are not cylindrical (not shown), and indicate that the electronic structures are three-dimensional rather than two-dimensional. This is consistent with the lack of anisotropic electronic transport and the electronic band structures.

Electronic conduction in the *zz* direction along the *c* axis in SrZrN$_2$ and SrHfN$_2$ should occur through the Sr layer. At the F point of the bottom of the conduction band, the Sr 4d$_{x^2-y^2}$ + 4d$_{xy}$ orbitals are involved in the *zz* direction electronic conduction, in addition to the Zr 4d$_{z^2}$ orbital. The orbital characters for the lowest conduction band in SrZrN$_2$ are shown in Figure 6. At the F point, the Zr d$_{z^2}$ orbital character is the most dominant, and the second and third most dominant are the Sr d$_{x^2-y^2}$ + d$_{xy}$ and Zr d$_{xz}$ + d$_{yz}$ orbitals, respectively. Figure 7 shows the partial density of states (DOS) near the bottom of the conduction band in SrZrN$_2$. The Sr d$_{x^2-y^2}$ + d$_{xy}$ orbital makes the third-largest contribution to the total DOS around the bottom of the conduction band, after the Zr d$_{z^2}$ and d$_{xz}$ + d$_{yz}$ orbitals. In SrHfN$_2$, the Sr d$_{x^2-y^2}$ + d$_{xy}$ orbital character dominates at the F point of the bottom of the conduction band, instead of the Hf d$_{z^2}$ orbital (Figures S7 and S8, Supporting Information). Usually, in SrMeO$_3$ perovskite oxides (Me = transition metal ion), the Sr 4d orbitals are at a higher energy level than the Me d orbitals.[29] In SrTiO$_3$, the lowest conduction band is formed by Ti 3d orbitals, with no contribution from the Sr 4d orbital.[30] In the perovskite oxide, SrZrO$_3$, the energy level of the Sr 4d t$_{2g}$ orbital (d$_{xy}$ + d$_{yz}$ + d$_{xz}$) is near that of the Zr 4d

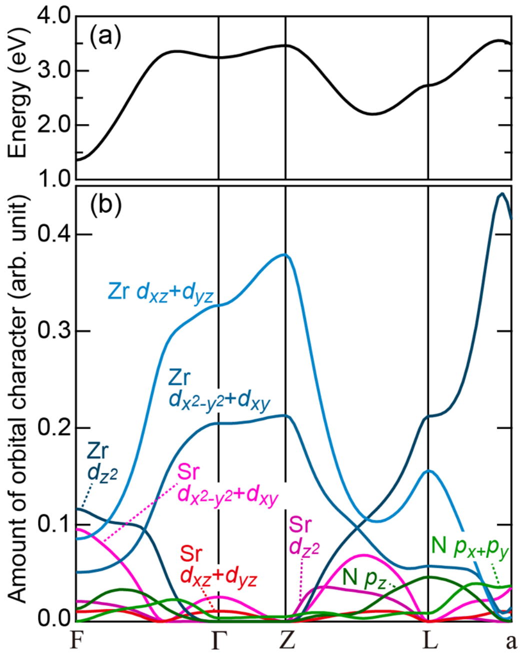

Figure 6. Orbital characters for the lowest conduction band of $SrZrN_2$. (a) Band dispersion for the lowest conduction band and (b) orbital characters for the lowest conduction band.

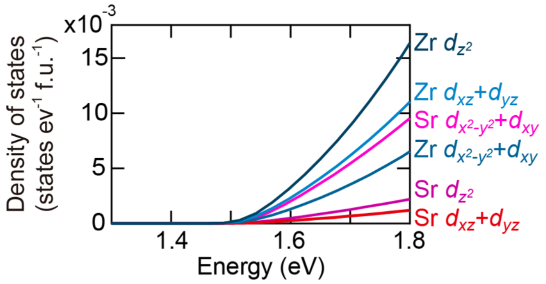

Figure 7. Partial DOS around the bottom of the conduction band in $SrZrN_2$.

t_{2g} orbital. The lowest conduction band in $SrZrO_3$ consists of Zr 4d t_{2g}, Sr 4d t_{2g}, and Sr 5s orbitals.[31,32] Because the energy levels of d^0 transition metal ions (Ti^{4+}, Zr^{4+}, Hf^{4+}) increase with the atomic number, the transition metal d-states are mixed with the Sr 4d-states in the lowest conduction band. Therefore, it is consistent that Sr $4d_{x^2-y^2}$ + $4d_{xy}$ orbitals and the Zr $4d_{z^2}$ (Hf $5d_{z^2}$) and Zr $4d_{xz}$ + $4d_{yz}$ (Hf $5d_{xz}$ + $5d_{yz}$) orbitals contribute to the *zz* direction electronic transport in $SrZrN_2$ and $SrHfN_2$. Such a three-dimensional electronic structure in layered compounds has also been found in metallic $LiMoN_2$,[33,34] which has a P3 layered crystal structure, and delafossite $PtCoO_2$ and $PdCoO_2$,[35−38] which have crystal structures related to the α-$NaFeO_2$ layered structure. In $PtCoO_2$ and $PdCoO_2$, the Pd 4d or Pt 5d orbitals of the A-site ion (Pt, Pd) layers contribute strongly to the *c* axis electronic conduction across the CoO_2 layer, similar to $SrZrN_2$ and $SrHfN_2$. The three-dimensional electronic structure means that a model in which the MN_2 layers only interact weakly is not adequate to describe these materials. These layers should interact across the Sr layer, resulting in a three-dimensional electronic band structure and isotropic electronic transport.

In comparison with $SrTiO_3$, the electronic conductivity and the electronic part of the *xx* direction (in-plane) thermal conductivities in $SrZrN_2$ and $SrHfN_2$ are lower than that in $SrTiO_3$. However, Seebeck coefficients in $SrZrN_2$ and $SrHfN_2$ reach -140 μV K^{-1} ($SrZrN_2$) and -145 μV K^{-1} ($SrHfN_2$) at 300 K, and -300 μV K^{-1} ($SrZrN_2$) and -370 μV K^{-1} ($SrHfN_2$) at 1200 K, and are larger than those of $SrTiO_3$ (-100 μV K^{-1} at 300 K, -160 μV K^{-1} at 1200 K) as shown in Figure 5 and S5 (Supporting Information). In addition to the electronic transport and Seebeck coefficient behavior, the temperature dependence of the power factors and electronic dimensionless figures of merit also vary. The power factors in $SrZrN_2$ and $SrHfN_2$ are slightly lower than that of $SrTiO_3$. However, the electronic dimensionless figures of merit of $SrZrN_2$ and $SrHfN_2$ are higher than $SrTiO_3$ over the entire temperature range. The calculated electronic dimensionless figures of merit for $SrTiO_3$ and $SrZrN_2$ are 0.4 and 0.47 at 300 K and 0.6 and 0.83 at 1200 K, respectively. Experimental figures of merit for $SrTiO_3$ are less than 0.1 at room temperature,[24,25] which is understandable, considering that lattice thermal conductivities are not included in the calculations. However, no experimentally determined and calculated thermal conductivities have been reported for $SrZrN_2$ and $SrHfN_2$. The experimentally measured thermal conductivities at room temperature of insulating compounds containing Sr and Zr or Hf ions are 1−5 W m^{-1} K^{-1} (4.06 W m^{-1} K^{-1} for $SrZrO_3$,[39] 1−5 W m^{-1} K^{-1} for ZrO_2,[40] 4.54 W m^{-1} K^{-1} for $SrHfO_3$,[41] 1−2 W m^{-1} K^{-1} for HfO_2[42]). These values are smaller than the thermal conductivities for $SrTiO_3$, which are around 10 W m^{-1} K^{-1}.[24,25] Therefore, lower thermal conductivities and larger dimensionless figures of merit can be expected in $SrZrN_2$ and $SrHfN_2$, although compared with $SrTiO_3$, the trends we have observed are promising.

■ CONCLUSIONS

We have calculated the electronic band structures and thermoelectric transport coefficients of the layered complex metal nitrides $SrZrN_2$ and $SrHfN_2$ using DFT and Boltzmann transport theory. $SrZrN_2$ and $SrHfN_2$ are band insulators with band gaps of 1.29 and 1.37 eV, respectively. They have three-dimensional electronic structures and isotropic transport properties, despite the α-$NaFeO_2$ layered crystal structure, because the bottom of the conduction bands are composed of Zr $4d_{z^2}$ (Hf $5d_{z^2}$), Zr $4d_{xz}$+$4d_{yz}$ (Hf $5d_{xz}$+$5d_{yz}$), and Sr $4d_{x^2-y^2}$+$4d_{xy}$ orbitals. Large Seebeck coefficients were found in both $SrZrN_2$ and $SrHfN_2$ and are larger than those for $SrTiO_3$, a well-known thermoelectric compound. There are many types of AMN_2 layered complex metal nitrides.[9] However, the number of known AMN_2 compounds is small compared with AMO_2 layered complex metal oxides. There may be many uncharacterized AMN_2 layered complex nitrides, which may exhibit novel physical properties. However, the synthesis of complex metal nitrides is often difficult. Recent epitaxial film growth techniques have overcome these problems, allowing single-phase samples to be synthesized.[43,44] The combination of electronic structure and transport calculations and these synthetic techniques should produce new AMN_2 layered compounds with excellent thermoelectric properties.

■ ASSOCIATED CONTENT

Ⓢ Supporting Information

Computational details, electronic structures, and thermoelectric transport properties of $SrHfN_2$. This material is available free of charge via the Internet at http://pubs.acs.org.

AUTHOR INFORMATION

Corresponding Author

*E-mail: OHKUBO.Isao@nims.go.jp.

Author Contributions

All authors have given approval to the final version of the manuscript.

Notes

The authors declare no competing financial interest.

ACKNOWLEDGMENTS

This work was supported by the Shorai Foundation for Science and Technology.

REFERENCES

(1) Koumoto, K., Mori, T., Eds.; *Thermoelectric Nanomaterials*; Springer: New York, 2013.

(2) Bednorz, J. G.; Muller, K. A. *Z. Phys. B* **1986**, *64*, 189−193.

(3) Kamihara, Y.; Watanabe, T.; Hirano, M.; Hosono, H. *J. Am. Chem. Soc.* **2008**, *130*, 3296−3297.

(4) Mizushima, K.; Jones, P. C.; Wiseman, P. J.; Goodenough, J. B. *Mater. Res. Bull.* **1980**, *15*, 783−789.

(5) Terasaki, I.; Sasago, Y.; Uchinokura, K. *Phys. Rev. B* **1997**, *56*, R12685−R12687.

(6) Takada, K.; Sakurai, H.; Takayama-Muromachi, E.; Izumi, F.; Dilanian, R. A.; Sasaki, T. *Nature* **2003**, *422*, 53−55.

(7) Singh, D. J. *Phys. Rev. B* **2000**, *61*, 13397−13402.

(8) Sugiura, K.; Ohta, H.; Nakagawa, S.; Huang, R.; Ikuhara, Y.; Nomura, K.; Hosono, H.; Koumoto, K. *Appl. Phys. Lett.* **2009**, *94*, 152105−1−152105−3.

(9) Gregory, D. H.; Barker, M. G.; Edwards, P. P.; Siddons, D. J. *Inorg. Chem.* **1996**, *35*, 7608−7613.

(10) Niewa, R.; DiSalvo, F. J. *Chem. Mater.* **1998**, *10*, 2733−2752.

(11) Yamanaka, S.; Hotehama, K.; Kawaji, H. *Nature* **1998**, *392*, 580−582.

(12) Blaha, P.; Schwarz, K.; Madsen, G.; Kvasicka, D.; Luitz, J. *WIEN2k, An Augmented Plane Wave + Local Orbitals Program for Calculating Crystal Properties*; TU Wien: Vienna, Austria, 2001.

(13) Tran, F.; Blaha, P. *Phys. Rev. Lett.* **2009**, *102*, 226401−1−226401−4.

(14) Koller, D.; Tran, F.; Blaha, P. *Phys. Rev. B* **2011**, *83*, 195134−1−195134−10.

(15) Guo, S. D.; Liu, B. G. *J. Appl. Phys.* **2011**, *110*, 073525−1−073525−5.

(16) Ohkubo, I.; Mori, T. *Chem. Mater.* **2014**, *26*, 2532−2536.

(17) Scheidemantel, T. J.; Ambrosch-Draxl, C.; Thonhauser, T.; Badding, J. V.; Sofo, J. O. *Phys. Rev. B* **2003**, *68*, 125210−1−125210−6.

(18) Madsen, G. K. H. *J. Am. Chem. Soc.* **2006**, *128*, 12140−12146.

(19) Madsen, G. K. H.; Singh, D. J. *Comput. Phys. Commun.* **2006**, *175*, 67−71.

(20) Chen, X.; Parker, D.; Singh, D. J. *Sci. Rep.* **2013**, *3*, 3168.

(21) Sevik, C.; Çağın, T. *Phys. Rev. B* **2010**, *82*, 045202−1−045202−7.

(22) Yang, J.; Li, H.; Wu, T.; Zhang, W.; Chen, L.; Yang, J. *Adv. Funct. Mater.* **2008**, *18*, 2880−2888.

(23) Robertson, J. *J. Vac. Sci. Technol., B* **2000**, *18*, 1785−1791.

(24) Okuda, T.; Nakanishi, K.; Miyasaka, S.; Tokura, Y. *Phys. Rev. B* **2001**, *63*, 113104−1−113104−4.

(25) Ohta, S.; Nomura, T.; Ohta, H.; Koumoto, K. *J. Appl. Phys.* **2005**, *97*, 034106−1−034106−4.

(26) Kinaci, A.; Sevik, C.; Çağın, T. *Phys. Rev. B* **2010**, *82*, 155114−1−155114−8.

(27) Usui, H.; Shibata, S.; Kuroki, K. *Phys. Rev. B* **2010**, *81*, 205121−1−205121−6.

(28) Nakamura, Y.; Uchida, S. *Phys. Rev. B* **1993**, *47*, 8369−8372.

(29) Lee, Y. S.; Lee, J. S.; Noh, T. W.; Byun, D. Y.; Yoo, K. S.; Yamaura, K.; Takayama-Muromachi, E. *Phys. Rev. B* **2003**, *67*, 11310−1−11310−4.

(30) Haverkort, M.; Zwierzycki, M.; Andersen, O. K. *Phys. Rev. B* **2012**, *85*, 165113−1−165113−20.

(31) Mete, E.; Shaltaf, R.; Ellialtioglu, S. *Phys. Rev. B* **2003**, *68*, 035119−1−035119−4.

(32) Evarestov, R. A.; Bandura, A. V.; Alexandrov, V. E.; Kotomin, E. A. *Phys. Status Solidi B* **2005**, *242*, R11−R13.

(33) Oliva, J. M.; Weht, R.; Ordejon, P.; Canadell, E. *Phys. Rev. B* **2000**, *62*, 1512−1515.

(34) Singh, D. J. *Phys. Rev. B* **1992**, *46*, 9332−9335.

(35) Tanaka, M.; Hasegawa, M.; Takei, H. *J. Phys. Soc. Jpn.* **1996**, *65*, 3973−3977.

(36) Eyert, V.; Fresard, R.; Maignan, A. *Chem. Mater.* **2008**, *20*, 2370−2373.

(37) Ong, K. P.; Zhang, S. T.; Wu, P. *Phys. Rev. B* **2010**, *81*, 115120−1−115120−6.

(38) Ong, K. P.; Singh, D. J.; Wu, P. *Phys. Rev. Lett.* **2010**, *104*, 176601−1−176601−4.

(39) Winter, M. R.; Clarke, D. R. *J. Am. Ceram. Soc.* **2007**, *90*, 533−540.

(40) Yamanaka, S.; Kurosaki, K.; Oyama, T.; Muta, H.; Uno, M.; Matsuda, T.; Kobayashi, S. *J. Am. Ceram. Soc.* **2005**, *88*, 1496−1499.

(41) Yamanaka, S.; Maekawa, T.; Muta, H.; Matsuda, T.; Kobayashi, S.; Kurosaki, K. *J. Solid State Chem.* **2004**, *177*, 3484−3489.

(42) Lee, S.-M.; Cahill, D. G.; Allen, T. H. *Phys. Rev. B* **1995**, *52*, 253−257.

(43) Luo, H.; Wang, H.; Bi, Z.; Feldmann, D. M.; Wang, Y.; Burrell, A. K.; McCleskey, T. M.; Bauer, E.; Hawley, M. E.; Jia, Q. *J. Am. Chem. Soc.* **2008**, *130*, 15224−15225.

(44) Luo, H.; Wang, H.; Bi, Z.; Zou, G.; McCleskey, T. M.; Burrell, A. K.; Bauer, E.; Hawley, M. E.; Wang, Y.; Jia, Q. *Angew. Chem., Int. Ed.* **2009**, *48*, 1490−1493.